VLM catecholaminergic neurons control tumor growth by regulating CD8$^+$ T cells

Ze Zhang[a,b,c], Yehua Li[b,c], Xueyuan Lv[b,c,d], Linlin Zhao[b,c,d], and Xiaodong Wang[b,c,1]

[a]College of Life Sciences, Beijing Normal University, Beijing 100875, China; [b]National Institute of Biological Sciences, Zhongguancun Life Science Park, Beijing 102206, China; [c]Tsinghua Institute of Multidisciplinary Biomedical Research, Tsinghua University, Beijing 100084, China; and [d]School of Life Sciences, Tsinghua University, Beijing 100084, China

Contributed by Xiaodong Wang, June 6, 2021 (sent for review February 21, 2021); reviewed by Liqun Luo and Jun Wang

It is known that tumor growth can be influenced by the nervous system. It is not known, however, if tumors communicate directly with the central nervous system (CNS) or if such interactions may impact tumor growth. Here, we report that ventrolateral medulla (VLM) catecholaminergic (CA) neurons in the mouse brain are activated in tumor-bearing mice and the activity of these neurons significantly alter tumor growth in multiple syngeneic and spontaneous mouse tumor models. Specific ablation of VLM CA neurons by a dopamine-β-hydroxylase (DBH) promotor-activated apoptosis-promoting caspase-3 in *Dbh-Cre* mice as well as inhibition of these neurons by a chemogenetic method slowed tumor progression. Consistently, chemogenetic activation of VLM CA neurons promoted tumor growth. The tumor inhibition effect of VLM CA neuron ablation is mitigated in *Dbh-Cre;Rag1*$^{-/-}$ mice, indicating that this regulatory effect is mediated by the adaptive immune system. Specific depletion of CD8$^+$ T cells using an anti-CD8$^+$ antibody also mitigated the tumor suppression resulting from the VLM CA neuron ablation. Finally, we showed that the VLM CA neuronal ablation had an additive antitumor effect with paclitaxel treatment. Collectively, our study uncovered the role of VLM CA neurons in the mouse brain in controlling tumor growth in the mouse body.

neuroimmunology | CA neurons | tumor model

There is accumulating evidence indicating that the interactions between the nervous and immune systems impact the body's response to many diseases, including cancer (1, 2), renal ischemia–reperfusion injury (IRI) (3), and allergic asthma (4). One such well-characterized interaction is the activation of the hypothalamus–pituitary–adrenal (HPA) axis that increases the levels of stress hormones like cortisol, epinephrine, and norepinephrine in the blood that negatively impact the immune system (5, 6). Additionally, the direct innervation of tumors and immune-related organs by sympathetic or parasympathetic nerve fibers has been shown to activate Wnt signaling in cancer stem cells to promote tumorigenesis, whereas unilateral or bilateral vagus nerve denervation of the pylorus attenuates gastric tumorigenesis (7). Similarly, denervation of sympathetic/adrenergic or parasympathetic/cholinergic nervous fibers in prostate tumors, respectively, slowed tumor formation or tumor metastasis (8). Moreover, there are speculations that specific neurons in the brain may response to and influence tumor growth in the body (1). However, which neurons in the central nervous system (CNS) may respond to tumor growth, and reciprocally, if such responses may influence tumor progression, are not clear.

Ventrolateral medulla (VLM) catecholaminergic (CA) neurons, also known as C1 neurons, are a group of catecholaminergic neurons located in the rostral ventrolateral medulla (9). This group of neurons has been identified as a key nodal point for stress in animals experiencing chronic restraint, endotoxin shock, and painful electric foot shocks (9, 10). Given the known influence of VLM CA neurons on the immune system in stress and inflammatory conditions (3, 11), we explored their potential influence on tumors.

In the current study, we utilized a *Cre*-dependent viral expression system to specifically induce apoptosis in VLM CA neurons. We also used viral-encoded chemogenetic tools to specifically activate or inhibit VLM CA neurons to study the function of this group of neurons in tumor initiation and progression in both syngeneic and spontaneous tumor models. We found that ablation or direct inhibition of this group of neurons slowed down tumor growth. Consistently, direct activation of these neurons promoted tumor growth. The impact of VLM CA neurons on tumor growth is mediated by the adaptive immune system, in particular, the cytotoxic CD8$^+$ T cells.

Results

Ablation of VLM CA Neurons Slowed Down Syngeneic Tumor Growth. Several previous studies have shown that chronic restraint stress promotes tumor growth in syngeneic breast and ovarian cancers, as well as spontaneously pancreatic cancer (12–14). Reciprocally, a study showed that tumor burden can induce depressive- and anxiety-like behaviors in the host animals, indicating that stress signals are somehow communicated between tumors and the brain (15). Given the known roles of VLM CA neurons in stress responses, we explored whether VLM CA neurons may somehow connect tumors and the brain. To this end, we inoculated murine colon adenocarcinoma MC-38 cells into immune-competent wild-type C57BL/6 mice and measured the activation of VLM CA neurons based on the expression of a neuronal activation marker c-Fos. Indeed, we found c-Fos expression in the VLM CA neurons after tumor inoculation while no such expression was observed for the phosphate-buffered saline (PBS)-inoculated (vehicle control) mice or naïve mice (Fig. 1*A*). Notably, this activation of VLM CA neurons by tumors was not restricted to MC-38 cells: the same group of neurons was also activated by inoculation with a different

Significance

We have discovered that the ventrolateral medulla (VLM) catecholaminergic (CA) neurons, a group of neurons that control mouse stress response, are activated in tumor-bearing mice, and the neuronal activity promotes tumor growth in multiple syngeneic and spontaneous mouse tumor models. The tumor-promoting effect of these VLM CA neurons is mediated by cytotoxic T cells. These findings establish an interaction between a tumor and a group of neurons in the mouse brain that influences tumorigenesis and tumor growth by modulating adaptive immunity.

Author contributions: Z.Z., Y.L., and X.W. designed research; Z.Z., Y.L., and L.Z. performed research; X.L. and L.Z. contributed new reagents/analytic tools; Z.Z., Y.L., and X.W. analyzed data; and Z.Z. and X.W. wrote the paper.

Reviewers: L.L., Stanford University; J.W., New York University.

The authors declare no competing interest.

[1]To whom correspondence may be addressed. Email: wangxiaodong@nibs.ac.cn.

This article contains supporting information online at https://www.pnas.org/lookup/suppl/doi:10.1073/pnas.2103505118/-/DCSupplemental.

Published July 6, 2021.

syngeneic mouse tumor cell line (Pan02) and by the spontaneously occurring tumors of $Apc^{min/+}$ mice (*SI Appendix*, Fig. S1*A*).

To study whether activated VLM CA neurons impact tumor growth, we first ablated VLM CA neurons by intracranial injection of Adeno-associated viruses (AAV)-double inverted orientation (DIO)-caspase 3 (Casp3) or AAV-DIO-mCherry (mCherry) virus into the VLM CA neuron-located brain regions of 2-mo-old *Dbh-Cre* mice (7). *Dbh-Cre* transgenic mice express the gene for the Cre enzyme under the control of the dopamine-β-hydroxylase (DBH) promoter (11). Since DBH functions in the biosynthesis of norepinephrine (a catecholamine) in VLM CA neurons, the VLM location-specific injection of AAV-Casp-3 virus encoding a fusion protein taCasp3-TEVp (tobacco etch virus protease, which cleaves and thereby activates caspase-3) can generate active caspase3 in DBH-expressing VLM CA neurons upon *Cre*-induced taCasp3-TEVp protein expression, causing host neuron apoptosis. As a negative control, AAV-mCherry virus was also injected into the same location of VLM CA neurons. The successful ablation of VLM CA neurons by AAV-Casp-3 was confirmed by staining brain slices from the mice 2 wk after virus injection. Overlapping signals for mCherry and TH (tyrosine hydroxylase, a marker for VLM CA neurons) were observed in AAV-mCherry–injected brains (Fig. 1*B*); no TH signal was observed in the AAV-Casp3–injected brain regions, indicating successful ablation of the VLM CA neurons. In contrast, TH signals were still present in the locus coeruleus (LC) and nuclear tractus solitaries (NTS) regions of those AAV-Casp3–injected brains (*SI Appendix*, Fig. S1*B*), confirming the precision of the injection as reported by a previous study (11).

To examine the impact of VLM CA neurons on tumor growth, we subcutaneously (s.c.) inoculated MC-38 tumor cells in the VLM CA neuron-ablated mice 2 wk after the AAV-Casp3 injection. We then measured tumor volumes every 3 d starting from day 6 after tumor inoculation using digital calipers (diagrammed in *SI Appendix*, Fig. S1*C*). Compared to the control (AAV-mCherry injected) mice, the VLM CA neuron-ablated mice displayed significantly slower tumor growth (Fig. 1*C*) and significantly decreased tumor size (Fig. 1 *D* and *E*). Monitoring of the survival rates of these animals revealed that the VLM CA neuron-ablated mice survived significantly longer with 7 out of 10 mice still alive 30 d after tumor inoculation compared to only 2 out of 10 survivors for the AAV-mCherry–injected control mice (Fig. 1*F*). Note that this tumor growth inhibition effect from VLM CA neuron ablation was also detected in male mice (*SI Appendix*, Fig, S1 *D–F*) and with an additional cancer cell line Pan02 (*SI Appendix*, Fig. S1 *G* and *H*).

Given that blood glucose contributes to the promotion of intestinal tumors (16) and pancreatic tumor growth (17), and considering that one of the known functions of VLM CA neurons is to regulate the blood glucose level under chronic stress conditions (11), we tested if the observed tumor growth difference after VLM CA neuron ablation was related to altered blood glucose levels. We observed no significant difference in blood glucose levels from week 1 to week 4 in control vs. VLM CA neuron-ablated mice after tumor inoculation (*SI Appendix*, Fig. S1*I*), indicating that the tumor growth inhibition from the VLM CA neuron ablation did not result from altered blood glucose levels.

The Activity of VLM CA Neurons Modulates Tumor Growth. Pursuing this initial observation that VLM CA neurons can impact tumor growth, we used the designer receptors exclusively activated by designer drugs (DREADD)-based chemogenetic method to selectively activate or inhibit this group of neurons in a controlled manner (18) and examined the ensuring impact on tumor growth. As diagrammed in *SI Appendix*, Fig. S2*A*, *Cre*-dependent AAV vectors encoding either the CA neuron-activating hM3D(Gq) receptor, or the CA neuron-inhibiting hM4D(Gi) receptor, were introduced to the VLM region of the mouse brain; this enabled host neuron activation or inhibition upon treatment of mice with clozapine-*N*-oxide (CNO), the known ligand for both hM3Dq and hM4Di.

We subsequently examined whether the activation or inhibition of VLM CA neurons using the hM3D(Gq) or hM4D(Gi) receptors affected tumor growth. We first injected AAV-DIO-hM3D(Gq) or AAV-DIO-hM4D(Gi) or AAV-DIO-mCherry control virus intracranially into 2-mo-old *Dbh-Cre* mice aimed at the VLM location. Two weeks after viral injection, we inoculated tumor cells subcutaneously into these mice and monitored tumor growth by digital caliper. After CNO exposure (in drinking water from day 1 of tumor inoculation), tumor growth was found to be faster in the hM3D(Gq)-expressing mice than in control AAV-mCherry–injected mice (Fig. 2*A*); conversely, the tumor growth of CNO-exposed hM4D(Gi)-expressing mice was significantly slower than the control AAV-mCherry–injected mice (Fig. 2*A*). At day 30 of tumor inoculation, the average tumor size in the VLM CA neuron-activated mice was about three times larger than tumors from the AAV-mCherry control mice and was about 20 times larger than the tumors from the VLM CA neuron-inhibited mice (Fig. 2*B* and quantified in Fig. 2*C*). Note that these differences in tumor growth rates were not due to CNO compound administration since tumor growth rates did not differ in *DBH-Cre* mice (without viral injections) with or without CNO in their drinking water (*SI Appendix*, Fig. S2*B*).

In addition to tumor weight and size, we also used an in vivo imaging system (IVIS) to measure tumor progression by inoculating mice with an MC38-derived cell line with stable luciferase expression (MC38-luc) (*SI Appendix*, Fig. S2*C*). As shown in Fig. 2*D* and quantified in Fig. 2*E*, the tumors of the VLM CA neuron-activated mice displayed much stronger photon intensity Fig. 2 *E* (*Left*) compared to the tumors of the VLM CA neuron-inhibited mice. Lastly, the survival rate analysis showed that the VLM CA neuron-inhibited mice had prolonged survival compared to the AAV-mCherry control mice (all 11 vs. 7 out of 10 survived after 30 d of tumor inoculation); and the VLM CA neuron-activated mice died sooner than the control mice (only 2 out 10 survival 30 d after tumor inoculation) (Fig. 2*F*). Collectively, these results demonstrated that direct activation of VLM CA neurons promoted tumor growth and that direct inhibition of VLM CA neurons slowed down tumor growth.

$CD8^+$ T Cells Are Required for VLM CA Neuronal Regulation of Tumor Progression. To explore the mechanism(s) underlying the differential tumor growth resulting from VLM CA neuronal manipulation, we crossed *Dbh-Cre* mice with $Rag1^{-/-}$ mice to generate *Dbh-Cre;*$Rag1^{-/-}$ mice. Consistent with a previous study (19), flow cytometry (FACS) analysis confirmed that the *Dbh-Cre;*$Rag1^{-/-}$ mice were T cell and B cell deficient (Fig. 3*A* and *SI Appendix*, Fig. S3*A*). We then injected AAV-Casp3 or AAV-mCherry into the CA neuronal region in these mice, followed by inoculation with MC-38 cells 2 wk after virus injection. The tumor size was measured from day 7 to day 22. Interestingly, we detected no inhibition of tumor growth upon VLM CA neuron ablation in the *Dbh-Cre;*$Rag1^{-/-}$ mice, indicating that the adaptive immune system is critical in the VLM CA neuron-mediated tumor growth effects we had earlier observed in immunocompetent *Dbh-Cre* mice (Fig. 3 *B* and *C* and *SI Appendix*, Fig. S3*B*). Consistently, we observed that in immunocompetent *Dbh-Cre* mice, there were significantly higher numbers of infiltrated $CD45^+$ leukocytes in their tumors following ablation of VLM CA neurons (Fig. 3*D* and *SI Appendix*, Fig. S3*C*). Profiling of these infiltrated $CD45^+$ leukocytes revealed increases in the $CD4^+$ and $CD8^+$ T cell populations (Fig. 3*E*). Notably, we also observed increased accumulation of $CD4^+$ and $CD8^+$ T cells in the spleens upon VLM CA neuron ablation after tumor inoculation (Fig. 3*F*).

We subsequently used antibodies against CD4 or CD8 to selectively deplete the $CD4^+$ or $CD8^+$ T cells in the *Dbh-Cre* mice after injection of AAV-Casp-3 or AAV-mCherry. Two weeks before MC-38 tumor cell inoculation, 2-mo-old mice were injected

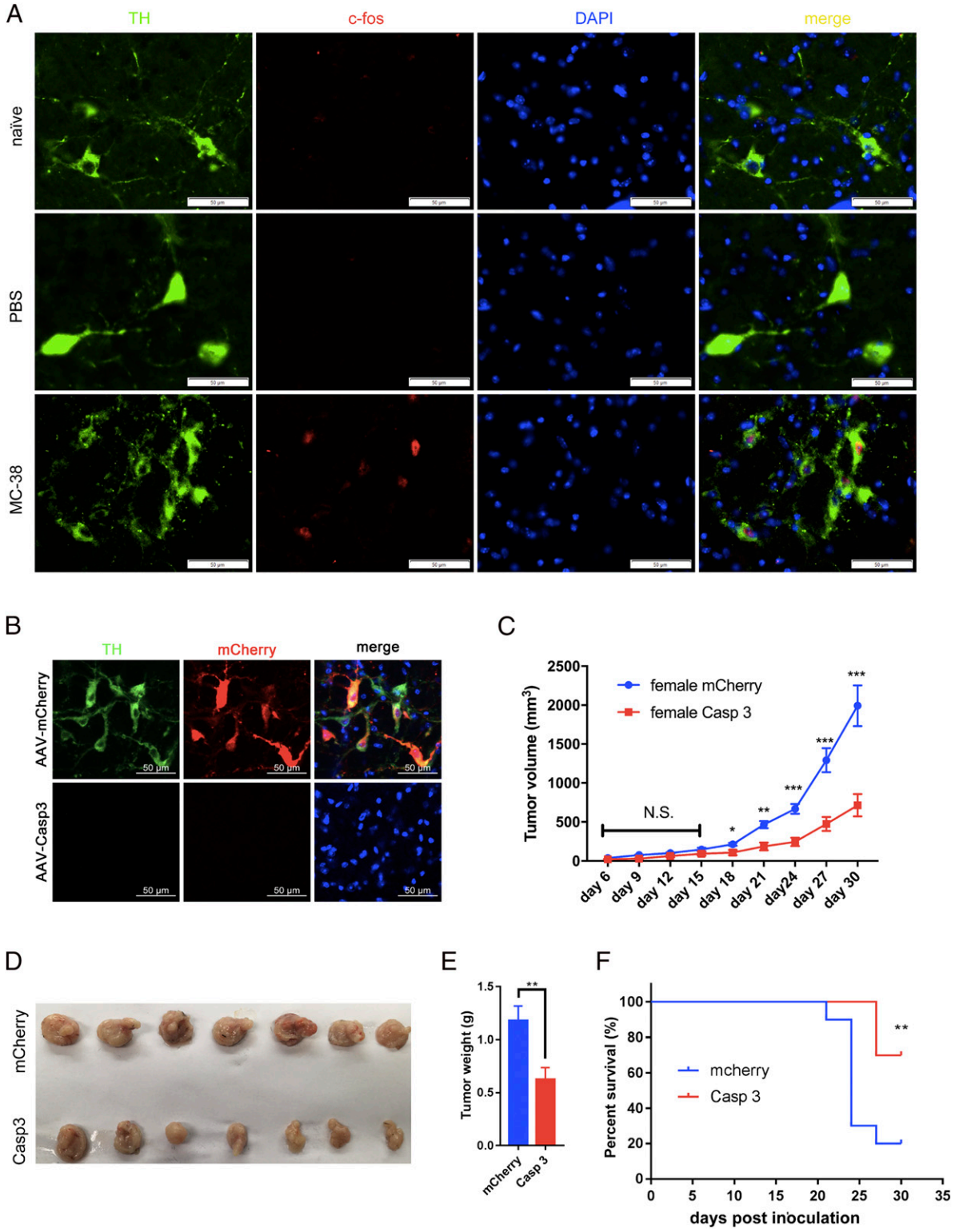

Fig. 1. Syngeneic mouse tumors activate VLM catecholaminergic neurons (VLM CA neurons) while depletion of VLM CA neurons slows tumor growth. (*A*) 1×10^6 MC-38 murine colon adenocarcinoma cells or vehicle (PBS) were inoculated into the flank of C57BL/6 mice. The tumor group displayed activation of neurons; such activation was not observed in the PBS or naive group. TH in green is a marker for VLM CA neurons; and *c-fos* in red is a marker of neuronal activation. TH and c-Fos double positive cell number in VLM CA: 8 ± 1 (naive) vs. 9 ± 2 (PBS) vs. 213 ± 10 (MC-38). (*B*) Specific ablation of VLM CA neurons by rAAV-taCasp3 virus-induced apoptosis. Control mice were injected with the rAAV-mCherry virus. The colocalization of mCherry and TH shows the accurate stereotactic manipulation, and the absence of a TH signal in the Casp3 group confirmed the ablation. TH positive cell number in VLM CA: 876 ± 46 (mCherry) vs. 63 ± 17 (Casp3). (*C*) The ablation of VLM CA neurons by AAV-taCasp3 slows syngeneic tumor growth. ($n_{Casp3} = 7$, $n_{mCherry} = 7$). (*D*) Images of the tumors from mCherry or Casp3 virus-injected mice. ($n_{Casp3} = 7$, $n_{mCherry} = 7$). (*E*) The ablation of VLM CA neurons reduces tumor weight. ($n_{Casp3} = 7$, $n_{mCherry} = 7$). (*F*) The ablation of VLM CA neurons extends the survival duration of mice. ($n_{Casp3} = 10$, $n_{mCherry} = 10$). Results shown represent the mean ± SEM. $^*P < 0.05$, $^{**}P < 0.01$, $^{***}P < 0.001$. See also *SI Appendix*, Fig. S1.

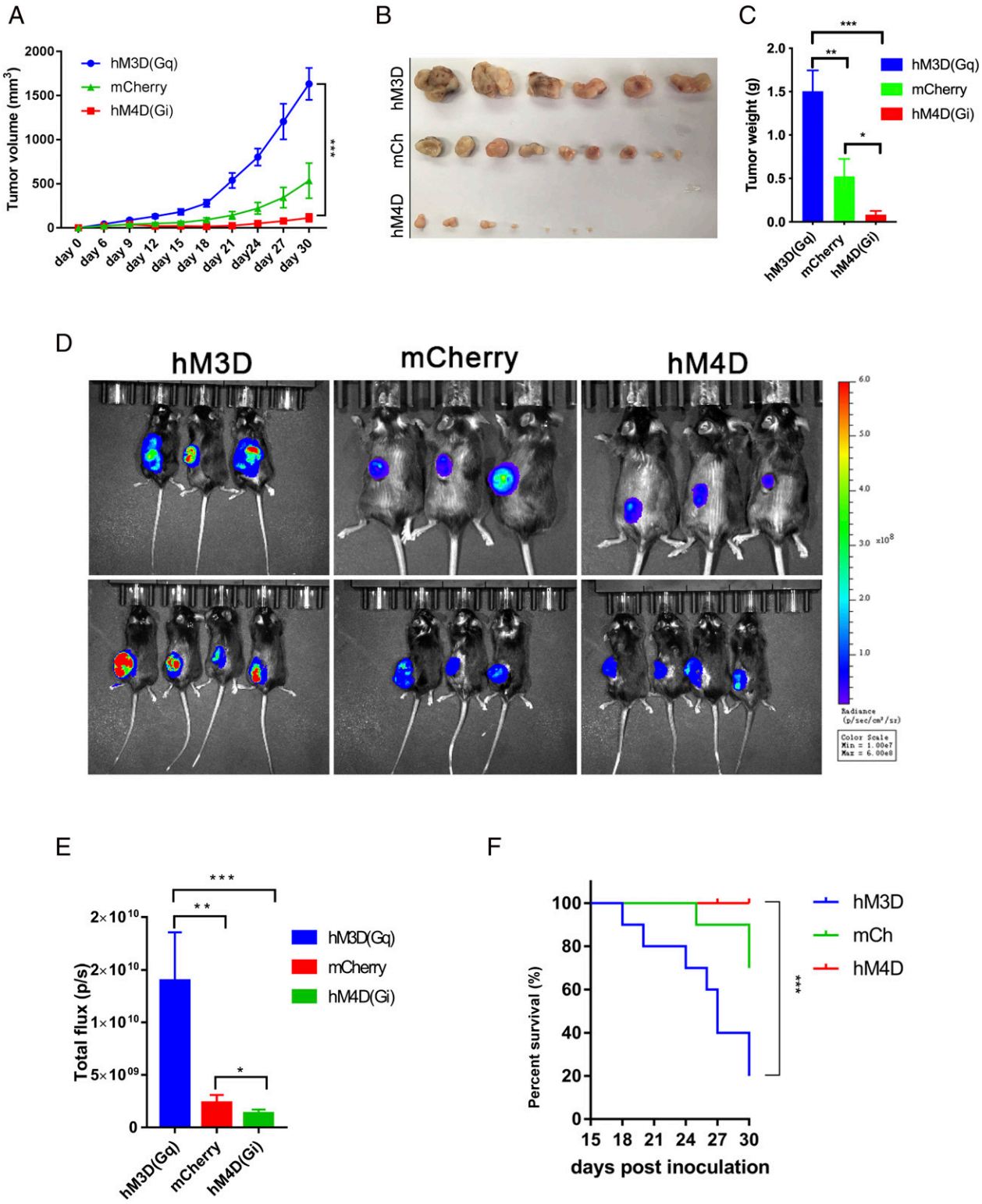

Fig. 2. The activity of VLM CA neurons controls tumor growth. (*A*) Tumor growth curve. The direct activation of VLM CA neurons by AAV-hM3D(Gq) can promote tumor growth; however, direct inhibition by AAV-hM4D(Gi) can slow tumor growth progression ($n_{hM3D} = 4$, $n_{mCherry} = 7$, $n_{hM4D} = 5$). (*B*) The tumor size image, obtained from dissected tumor-bearing mice, showing that activation of VLM CA neurons can enhance tumor size, and that inhibition of VLM CA neurons can reduce tumor size ($n_{hM3D} = 6$, $n_{mCherry} = 9$, $n_{hM4D} = 7$). (*C*) The tumor weight showing the tumor promotion impact from the activation of VLM CA neurons and the tumor inhibition impact upon inhibition of VLM CA neurons ($n_{hM3D} = 6$, $n_{mCherry} = 9$, $n_{hM4D} = 7$). (*D*) IVIS imaging. In vivo imaging showing VLM CA neuron activation [by AAV-hM3D(Gq)] results in relatively stronger photon intensity, whereas inhibition of VM CA neurons by AAV-hM4D(Gi) results in relatively weaker photon intensity ($n_{hM3D} = 3$, $n_{mCherry} = 3$, $n_{hM4D} = 3$). (*E*) Histogram showing the quantified IVIS results ($n_{hM3D} = 3$, $n_{mCherry} = 3$, $n_{hM4D} = 3$). (*F*) Survival curve. Inhibition of VLM CA neuron activity by AAV-hM4D(Gi) can prolong survival while VLM CA neuron activation by AAV-hM3D(Gq) can accelerate the time to death for tumor-bearing mice ($n_{hM3D} = 10$, $n_{mCherry} = 10$, $n_{hM4D} = 11$). Results shown represent the mean ± SEM $^*P < 0.05$, $^{**}P < 0.01$, $^{***}P < 0.001$.

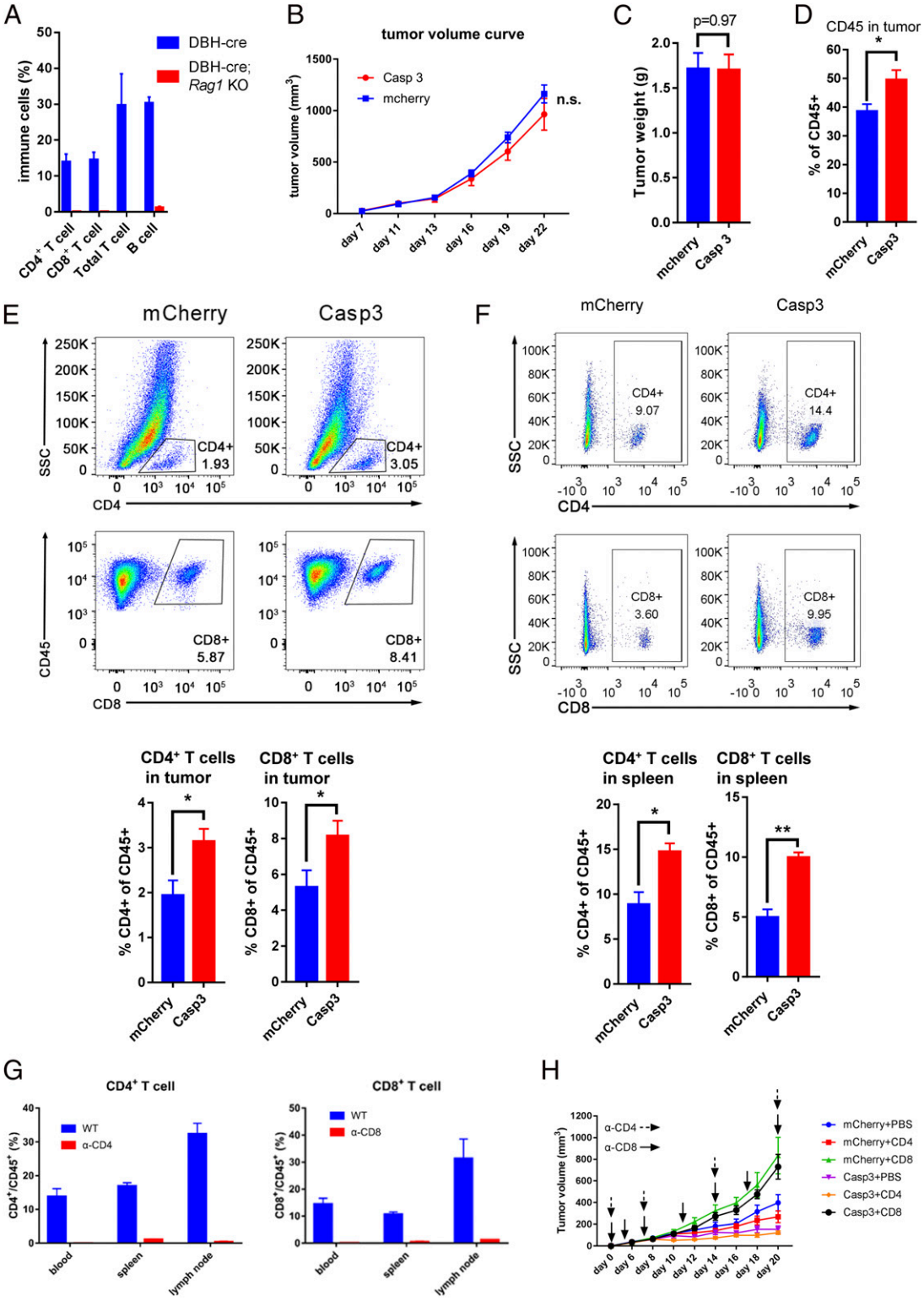

Fig. 3. The adaptative immune system functions in VLM CA neuron-regulated tumor growth. (*A*) Quantification of FACS for $CD4^+$ and $CD8^+$ T cells in *Dbh-Cre;Rag1*$^{-/-}$ mice. The *Dbh-Cre;Rag1*$^{-/-}$ mice ($n_{Dbh\text{-}Cre}$ = 3, $n_{Dbh\text{-}Cre;Rag1^{-/-}}$ = 3) had no $CD4^+$, $CD8^+$ T cells, total T cells and B cells. (*B* and *C*) There were no differences observed in tumor weight between the AAV-mCherry– vs. AAV-Casp3–treated immunodeficient *Dbh-Cre;Rag1*$^{-/-}$ mice (n_{Casp3} = 8, $n_{mCherry}$ = 14). (*D*) There was more leukocyte infiltration indicated by $CD45^+$ cells after VLM CA neuron ablation compared with mCherry control mice (n_{Casp3} = 6, $n_{mCherry}$ = 6). There were more $CD4^+$ and $CD8^+$ T cells after VLM CA neuron ablation intratumor (*E*) and in spleen (*F*) (n_{Casp3} = 6, $n_{mCherry}$ = 6) after tumor inoculation. (*G*) The successful depletion of $CD4^+$ and $CD8^+$ T cells based on $CD4^+$ or $CD8^+$ T depletion antibodies, respectively (n_{Casp3} = 3, $n_{mCherry}$ = 3). (*H*) It was $CD8^+$ T cells that functioned in VLM CA regulated tumor growth process mCherry + PBS vs. Casp3 + PBS, $P = 0.004$; mCherry + PBS vs. mCherry + CD4, $P = 0.179$; mCherry + PBS vs. mCherry + CD8, $P = 0.027$; Casp3 + PBS vs. Casp3 + CD4, $P = 0.398$; Casp3 + PBS vs. Casp3 + CD8, $P = 0.000$; mCherry + CD4 vs. Casp3 + CD4, $P = 0.011$; mCherry + CD8 vs. Casp3 + CD8, $P = 0.618$ ($n_{mCherry+PBS}$ = 12, $n_{mCherry+CD4}$ = 12, $n_{mCherry+CD8}$ = 12, $n_{Casp3+PBS}$ = 14, $n_{Casp3+CD4}$ = 14, $n_{Casp3+CD8}$ = 12). Results shown represent the mean ± SEM $^*P < 0.05$, $^{**}P < 0.01$, $^{***}P < 0.001$.

with the appropriate AAV. The mice were given intraperitoneal injection of the $CD4^+$ or $CD8^+$ T cell depleting antibodies. The antibody injection frequency was once per week for the CD4 depleting antibody and twice per week for the CD8 depleting antibody as previously described (20–23). Successful elimination of $CD4^+$ or $CD8^+$ T cells was confirmed by FACS analysis of the peripheral blood, spleens, and lymph nodes of these animals (Fig. 3*G* and *SI Appendix*, Fig. S3*D*). Interestingly, $CD4^+$ T cell depletion only modestly influenced tumor growth, whereas $CD8^+$ T cell depletion largely eliminated any tumor growth inhibition from VLM CA neuron ablation (Fig. 3*H*). These results suggest that VLM CA neurons mediate tumor growth regulation mainly via $CD8^+$ T cells.

Ablation of VLM CA Neurons Slowed the Tumor Progression of Spontaneously Occurring Tumors. Having observed these VLM CA neuron-mediated effects on the progression of syngeneic tumors, we further studied the potential impacts of VLM CA neurons on spontaneously occurring tumors. We conducted experiments using two spontaneously occurring tumor models ($APC^{min/+}$ and azoxymethane [AOM]/ dextran sulfate sodium [DSS] mice models) and found that VLM CA neuron ablation from $APC^{min/+}$ mice caused significant reductions in both the overall number of polyps and the mean polyp diameter (Fig. 4 *A*–*C*). The polyp incidence in colons of $APC^{min/+}$ mice decreased from 100% (9/9) to 50% (3/6) after VLM CA neuron ablation (*SI Appendix*, Fig. S4*A*). There was also obvious alleviation of tumor burden in these mice after VLM CA neuron elimination (Fig. 4*D*).

With the AOM/DSS tumor model, we first introduced AAV-Casp3 or control AAV-mCherry into the CA neuron-located brain region of 2-mo-old *DBH-Cre* mice and started feeding the viral-injected mice with AOM followed by 2.5% DSS-containing water for a consecutive window of 5 d, one in each 19-d period (diagrammed in *SI Appendix*, Fig. S4*B*). The mice were killed after 80 d (after three DSS feeding windows). Histological analysis showed the typical lymphoid aggregate, inflammatory infiltrate, polyp, and tubular adenoma, supporting successful establishment of this tumor model. The body weights of the VLM CA neuron-ablated mice were slightly higher than the control mCherry mice, an observation indirectly indicating the protective effects of VLM CA neuronal ablation in this model (*SI Appendix*, Fig. S4*C*). Indeed, we found that the percentage of larger tumors was significantly lower in VLM CA neuron-ablated mice than in the AAV-mCherry control mice (Fig. 4*E*).

Finally, we examined whether VLM CA neuronal ablation could enhance the efficacy of systemic chemotherapy in treating colon cancer. In this experiment, AAV-Casp3 or AAV-mCherry virus was specifically introducted into the VLM CA brain region of *Dbh-Cre* mice (2 mo). Two weeks after viral injection, the animals were inoculated with the MC-38 tumor cell line. When the tumors in both groups reached about 100 mm^3, systematic administration of paclitaxel (also known as taxol) or PBS was given to these animals. Interestingly, the taxol-treated mice with ablated VLM CA neurons displayed a significantly greater extent of tumor growth inhibition than the mice given taxol but with their VLM CA neurons undisturbed (Fig. 4*F*), without affecting the body weight of these animals during the treatment period (*SI Appendix*, Fig. S4*D*). Together, these findings suggest that the combination of VLM CA neuronal manipulation and chemotherapy taxol has an enhanced inhibitory effect on tumor growth.

Discussion

There are now studies supporting the notion that various neuronal activities can regulate tumorigenesis, tumor progression, efficacy of cancer treatments, and overall cancer patient prognosis (1). Moreover, it is becoming increasingly clear that tumor burden may influence nervous system functions. Such bidirectional interactions between the nervous system and tumors is now becoming a fast growing research field known as cancer neuroscience (1). Stress response in the brain might be the central nodule that connects the tumor growth and neuronal response to tumors. VLM CA neurons are known to function as a convergence point for stress information and have been implicated in antiinflammation responses, blood glucose regulation, blood pressure, cardiovascular homeostasis, arousal, and sleep (3, 11, 24). Our work in the present study suggests that these neurons also participate in tumor growth regulation.

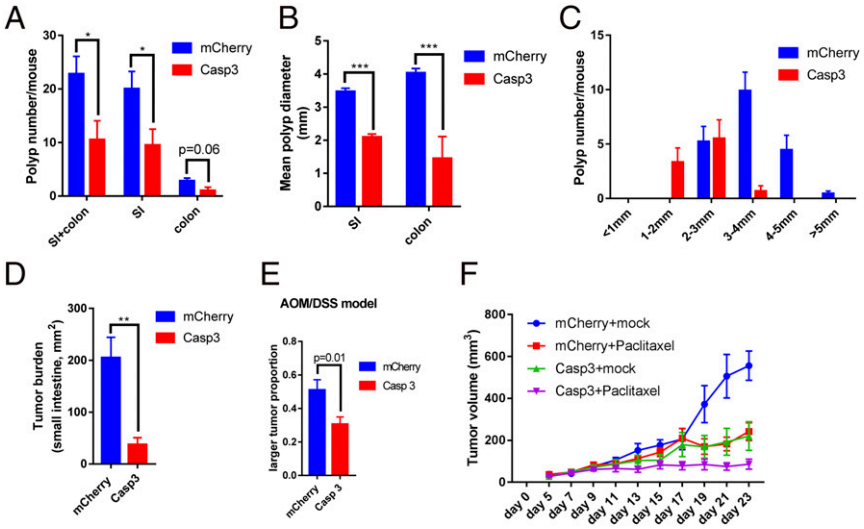

Fig. 4. VLM CA neuron ablation slows down tumor progression spontaneously. There are fewer (*A*) and smaller (*B*) polyps in mouse intestine (including small intestine and colon) by using the *Dbh-Cre;*$APC^{min/+}$ mice model after VLM CA neuron ablation. SI, small intestine. (*C*) The smaller polyps (<3 mm) were dominant after VLM CA neuron ablation, and the larger polyps (>3 mm) were dominant in control mCherry-introduced mice ($n_{Casp3} = 6$, $n_{mCherry} = 9$). (*D*) There was decreased tumor burden after VLM CA neuron ablation by using the $APC^{min/+}$ mice model. (*E*) There were fewer large polyps (>3 mm) in colons after VLM CA neuron ablation by using the AOM/DSS model. ($n_{Casp3} = 6$, $n_{mCherry} = 6$). (*F*) There were additive effects of taxol (paclitaxel) and VLM CA neuron manipulation in the MC-38 inoculation mouse model. ($n_{mCherry+mock} = 12$, $n_{mCherry+Paclitaxel} = 12$, $n_{Casp3+mock} = 12$, $n_{Casp3+Paclitaxel} = 14$). Results shown represent the mean ± SEM $^*P < 0.05$, $^{**}P < 0.01$, $^{***}P < 0.001$.

The effect of VLM CA neurons on tumor growth seems to be mediated by the adaptive immune system, particularly $CD8^+$ T cells, since such an effect was mitigated in *Rag1*$^{-/-}$ mice or in mice in which the $CD8^+$ T cells were depleted with an antibody. However, the experiments were done only with MC-38 tumor cells. It is thus possible that other immune cells, including Treg cells and macrophages, are also involved in VLM CA neuron-regulated tumor growth in other tumor models, including the spontaneous tumor models.

How tumors communicate with the VLM CA neurons in the brain and how the neuronal activity of VLM CA neurons influence the adaptive immune system are not currently known. However, unlike the previously characterized direct innervation of tumors or immune-related organs by sympathetic or parasympathetic nerve fibers, the relationship(s) between VLM CA neurons and tumors and/or the immune system must be indirect, since the projection of these neurons does not go into peripheral tissues (3, 9–11). It is thus interesting to speculate that the cancer-related VLM CA neuronal function may be mediated by neuron-derived "factors" that 1) are able to cross the blood brain barrier and can be perceived by the adaptive immune system and/or tumor cells, or 2) the CA neuron projection can be relayed to the adaptive immune system and/or tumor tissues by secondary neurons. The reciprocal relationship—i.e., how tumors activate VLM CA neurons—is probably even more mysterious. The specific activation of this one neuronal subset in one brain region would suggest that some projection input(s) or a receptor protein(s) unique to these cells may participate in this activation. Having now established these activated neurons as a readout upon tumor inoculation (with multiple cancer models), it is now possible to address these questions experimentally.

We currently have several hypotheses about possible mechanisms through which VLM CA neurons can be activated and about how VLM CA neurons may control the population of T cells. Several upstream inputs into VLM CA neurons have been reported, including from the paraventricular nucleus (PVN), the lateral parabrachial nucleus (LPB), the lateral hypothalamus (LH), the nucleus tractus solitaries (NTS), the periaqueductal gray (PAG), the dorsal raphe nucleus (DRN), the dorsomedial hypothalamic nucleus (DMH), the bed nucleus of the stria terminalis (BNST), and the central amygdaloid nucleus (CeA), among others (11). To examine their activation systematically in tumor-bearing mice should further map this neural circuit and identify the upstream neurons that perceive the tumor presence in the body.

As for how VLM CA neurons regulate the immune system, there are previous studies demonstrating that the HPA axis might be regulated by VLM CA neurons (9), and this axis is known to modulate the immune system by releasing norepinephrine, epinephrine, and glucocorticoids, among others (25, 26). Consistent with this idea, we detected a significant decrease in the stress hormone levels in mice when their VLM CA neurons were ablated (*SI Appendix*, Fig. S4*F*), suggesting that the suppressed immune response to tumors by the stress hormones might be liberated by VLM CA neurons ablation (27–30). However, whether the change in these immune-modulating stress hormones is solely responsible for the VLM CA neuronal effect on tumor growth remains to be validated.

There could also be a brain–gut axis through which the VLM CA neurons could influence microbiota, which may subsequently modulate an individual's immune system to regulate tumor growth (31). A previous study showed that chronic stress promotes DSS-induced colitis by disturbing the gut microbiota and triggering immune system response (32). All these possibilities should be exciting topics for future studies.

Once the mechanisms are discovered through which tumors communicate with VML CA neurons and VML CA neurons communicate with the adaptive immune system, it will be tempting to speculate that specific modulation of these interactions could complement existing chemotherapy, targeted therapy, and immune therapy for cancer.

Materials and Methods

Mice. All animal experiments were conducted following the Chinese Ministry of Health national guidelines for the housing and care of laboratory animals; moreover, they were reviewed and approved by, and performed in accordance with, the Institutional Animal Care and Use Committee of the National Institute of Biological Sciences, Beijing. All the mice were housed in groups of five per cage under specific-pathogen free (SPF) conditions and maintained with a 12/12 light/dark cycle at 22 to 25 °C with food and water ad libitum. Wild-type C57BL/6 (hereafter termed B6), *Dbh-Cre*, *Rag1*$^{-/-}$, and *Apc*$^{min/+}$ mice were used in this study. B6 mice were purchased from Vital River Laboratory Animal Technology Co. The *Dbh-Cre* [Tg(Dbh-cre)KH212Gsat/Mmcd] were originally obtained from the Mutant Mouse Resource and Research Centers (MMRRC) and maintained on a B6 background. *Rag1*$^{-/-}$ mice were kindly provided by Chen Dong at Tsinghua University. *Apc*$^{min/+}$ mice were kindly provided by Rongwen Xi at the National Institute of Biological Sciences (NIBS). We generated *Dbh-Cre;Rag1*$^{-/-}$, *Dbh-Cre;Apc*$^{min/+}$ mice by crossing *Dbh-Cre* and *Rag1*$^{-/-}$ or *Apc*$^{min/+}$ mouse lines, respectively. Both male and female mice (aged 6 to 8 wk) were used in this study. When relevant and applicable, age-matched mice were randomly chosen from the same cages to be included in experimental and control groups. All mice were genotyped by using a One Step Mouse Genotyping Kit (Vazyme Biotech Co. Ltd.)

The following two primer pairs were used for *Dbh-Cre* transgenic mice genotyping: Dbh-F: 5′-AATGGCAGAGTGGGGTTGGG-3′ and CreGS-R: 5′-CGGCAAACGGACAGAAGCATT-3′; Cre-F: 5′-ACGAGTGATGAGGTTCGCAAG-3′ and Cre-R: 5′-ATTAACATTCTCCCACCGTCAGT-3′.

The following primers were used for *Rag1*$^{-/-}$ mice genotyping: 23267: 5′-TCTGGACTTGCCTCCTCTGT-3′, 23268: 5′-CATTCCATCGCAAGACTCCT-3′, oIMR8162: 5′-TGGATGTGGAATGTGTGCGAG-3′. The following primers were used for *Apc*$^{min/+}$ mice genotyping: IMR0034: 5′-TTCCACTTTGGCATAAGGC-3′ and IMR0758: 5′-TTCTGAGAAAGACAGAAGTTA-3′

Cell Lines. MC-38 and Pan02 cell lines were used in this study. MC-38, a murine colon adenocarcinoma cell line, was kindly provided by Zhirong Shen and Bin Jiang, BeiGene (Beijing, China). Pan02, a mouse pancreatic ductal adenocarcinoma cell line, was kindly provided by Jianhua Sui, NIBS (Beijing, China). MC-38 cells were cultured in Dulbecco's Modified Eagle Medium (Gibco) supplemented with 10% fetal bovine serum (FBS) (Gibco), 1% penicillin/streptomycin (Pen/Strep) (Gibco), 2 mM glutamine, 0.1 mM nonessential amino acids, 1 mM sodium pyruvate, 10 mM Hepes, and 50 μg/mL gentamicin sulfate. The Pan02 cell line was cultured in RPMI-1640 medium supplemented with 10% FBS. All cells were cultured at 37 °C in an incubator with a 5% CO_2 atmosphere. MC-38 cells stably expressing luciferase ("MC38-luc") were generated by infecting with pHBLV-CMV-MCS-fLUC-EF1α-ZsGreen-T2A-Puro virus; the luciferase lentiviruses were obtained from HanBio Technology (Shanghai, China). We regularly checked all of the cell lines to confirm they were negative for *Mycoplasma* by PCR-based assay, using the following primers: Myco-F: 5′-GGGAGCAAACAGGATTAGATACCCT-3′ and and Myco-R: 5′-TGCACCATCTGTCACTCTGTTAACCTC-3′ (33).

Blood Glucose Measurement. Following a previous study (11) the end of mouse tails were cut horizontally with a razor blade, and a small drop of blood was collected via gentle massage. The glucose level was then measured using a blood glucose meter (One Touch, Johnson & Johnson Medical). No food was supplied during the blood glucose measurement period.

Quantification of Norepinephrine, Epinephrine, and Corticosterone in Mouse Serum. Mouse blood samples were collected, and then serum was prepared by centrifugation for 10 min at 4,000 rpm at 4 °C. Commercial ELISA kits from Sbjbio were used for measuring serum NE (norepinephrine), E (epinephrine), and corticosterone levels, following the manufacturer's instructions.

Tumor Growth and Treatment. Tumor cells were injected s.c. on the flank of mice. Mice were randomized into treatment groups when the tumors reached predetermined sizes. MC-38 tumor-bearing mice received intraperitoneal (i.p.) administration of paclitaxel (TargetMol). Tumor volumes were measured for length (a) and width (b), and the tumor volume was calculated as $0.5326 \times a \times b^2$. For the survival curve, the mice were inoculated with 2×10^6 cells, and if each length and width of the tumor was >20 mm or the tumor volume was >2,000 mm^3, the mice were considered dead.

In Vivo Depletion of Immune Cells. For antibody depletion experiments, mice received i.p. administration of CD4 depletion antibody (anti-CD4 mAb GK1.5) at a dose of 1 mg/mL, 0.2 mL/mouse, once/week, or CD8 depletion (anti-CD8 mAb 2.43) antibody at a dose of 1 mg/mL, 0.2 mL/mouse, twice/week. The anti-CD4 mAb GK1.5 was purchased from Bio X Cell, and anti-CD8 mAb 2.43 was produced following the patent described in the NIBS Antibody Center.

IVIS Analysis. Luciferase-expressing tumor cells were injected s.c. on the flank of the mice. In vivo bioluminescence imaging was performed using an IVIS imaging system (PerkinElmer) by i.p. injection of luciferin (GoldBio). After anesthetization with 2% isofluorane and injection of 150 mg/kg luciferin, mice were photographed under brightfield, and images were overlaid with luminescence data gathered over the maximum exposure period without pixel saturation (0.5 to 60 s).

Flow Cytometry Analysis and Cell Sorting. Samples of tumor, spleen, lymph node, and blood were harvested after killing the mice. Single-cell suspensions of tumors were obtained using a Tumor Dissociation Kit (Miltenyi). The single cells were then incubated in MACS buffer (PBS supplemented with 2% FBS and 1 mM ethylenediaminetetraacetic acid [EDTA]) containing 10 μg/mL CD16/CD32 antibody (2.4G2, BD PharMingen) for 30 min at 4 °C and then stained with the antibodies. Staining reagents included anti-CD45 (30-F11, BioLegend), anti-CD45 (30-F11, BioLegend), anti-CD3 (17A2, BioLegend), anti-CD3 (17A2, BioLegend), anti-CD4 (RM4-5, BioLegend), anti-CD8a (53-6.7, BioLegend), anti-CD25 (PC61, BioLegend), anti-CD44 (IM7, BioLegend), and anti-CD62L (MEL-14, BioLegend). Data were collected on an BD FACSAria Fusion flow cytometer and analyzed with FlowJo software (TreeStar). Dead cells and cell aggregates were excluded from analyses based on a LIVE/DEAD Fixable Near-IR Dead Cell Stain Kit (eBioscience), or DAPI, with forward scatter/side scatter characteristics. The immune cell gating strategy was as follows: T cell: $CD45^+$ $CD3^+$, $CD4^+$ T cell: $CD45^+$ $CD3^+$ $CD4^+$, $CD8^+$ T cell: $CD45^+$ $CD3^+$ $CD8^+$, B cell: $CD45^+$ $CD3^-$ $CD19^+$.

Immunohistochemistry, Immunofluorescence, and Histology. For tissue section, after deeply anesthetized and intracardial perfusion with PBS and 4% paraformaldehyde (PFA) in PBS, tissues were postfixed in 4% PFA overnight at 4 °C, then dehydrated in 20% and 30% sucrose for cryoprotection, and then all samples were embedded in optimal cutting temperature compound (Tissue-Tek), and flash frozen in liquid nitrogen. Brain slices (20 to 30 μm in thickness) were cut using a cryostat (Leica). For immunofluorescence staining, slides were blocked and permeabilized with superblock blocking buffer (Thermo Scientific) supplemented with 0.1% Triton X-100 for 40 to 60 min at room temperature and then incubated with primary antibodies in phosphate buffered saline with Tween-20 (PBST) buffer in a humidified chamber at 4 °C overnight. Primary antibodies include tyrosine hydroxylase (Abcam) and c-Fos (Abcam). After staining with primary antibodies, the tissue slices were washed three times with PBST and incubated with fluorochrome-conjugated secondary antibodies at room temperature for 1 to 2 h in the dark with gentle agitation. Secondary antibodies included AF488 donkey anti-chicken (Jackson ImmunoResearch), AF555 donkey anti-rabbit (Invitrogen), and AF647 donkey anti-rabbit (Jackson ImmunoResearch) for 60 min at room temperature. After washing three times with PBST, the tissues slices were mounted with 50% glycerol mounting medium with DAPI. Images were examined using an Olympus VS120 or Zeiss LSM800 confocal microscope.

Stereotactic Viral Microinjection. Mice were anesthetized with Avertin (intraperitoneal, 20 mg/mL working solution prepared with 2,2,2-tribromomethanol and tertamyl alcohol, 0.2 mL Avertin per 10 g mice) and placed into a stereotaxic apparatus. The skin was cut, and a small craniotomy was made in the skull. Using a syringe (Hamilton syringe, 1700 series), AAV virus (500 nL) was slowly injected into the VLM CA (coordinate anteroposterior/dorsoventral/mediolateral: −7.5/−5.0/±1.2 mm) under pressure. To selectively ablate the subpopulation of VLM CA, a *Cre*-dependent AAV-Casp3 virus (rAAV-flex-taCasp3-TEVp-WPRE-pA; AAV2/9) was bilaterally injected into the *Dbh-cre* and *Dbh-Cre;Rag1*$^{-/-}$. As a control, a *Cre*-dependent AAV-mCherry virus (rAAV-EF1α-DIO-mCherry-WPRE-pA;AAV2/9) was also injected using the same procedure.

For the chemogenetics experiments, hM3D virus [rAAV-hSyn-DIO-hM3D(Gq)-mCherry-WPRE-pA;AAV2/9], hM4D [rAAV-hSyn-DIO-hM4D(Gi)-mCherry-WPRE-pA;AAV2/9], or mCherry control virus (rAAV-EF1α-DIO-mCherry-WPRE-pA;AAV2/) were injected into VLM CA neurons to directly activate or inhibit neuron activity. After that the mice intraperitoneally received 1.0 mg/kg CNO (MedChemExpress) every day. To maintain the activity or inhibition of VLM CA neurons, the mice were maintained with drinking water that was supplemented with 1.25 mg/kg CNO, assuming water consumption of 5 mL per day.

All AAV viruses were purchased from BrainVTA in Wuhan, China, and the virus titers were $\sim 1 \times 10^{12}$ vg/mL.

AOM/DSS Induced Colitis-Associated Colon Cancer Model (CAC). The CAC model was modified from a previous study (34, 35). Briefly, 2 wk after stereotactic viral injection into the VLM CA neurons of 2-mo-old mice, sex-matched mice were i.p. injected with 8.0 mg/kg of AOM (Sigma-Aldrich). After 5 d, the mice were treated with 2.5% DSS (MP Biomedicals, molecular weight 36 to 50 kDa) in drinking water for 5 d. The mice then underwent 14 d of recovery during which the DSS water was replaced with regular water. This cycle was repeated three times, altering the 2.5% DSS water with 2.0% DSS water. On day 80, mice were killed and processed for tumor analysis. In all experiments, littermate controls were used to enable comparison with mice of the same genetic background. The animals that exhibited health concerns unrelated to the study conditions were excluded from the analysis. The animals were blindly monitored daily or twice per week by weighing and clinical scoring during AOM/DSS treatment. Polyp burden was calculated as the sum of the volumes of all tumors in a given mouse (volume = 1/2 × radius^2).

Statistical Analysis. All data are presented as the mean ± SEM, unless specifically noted otherwise. Statistics and graphing were conducted in GraphPad Prism 7 software. Statistical analyses were performed using a two-tailed, unpaired Student's *t* tests. Tumor growth after different treatments was analyzed by two-way ANOVA. The survival curves were generated by the Kaplan–Meier method. A *P* value of less than 0.05(*), 0.01(**), or 0.001(***) was considered statistically significant. Representative data show the results from two to three independent experiments.

Data Availability. All study data are included in the article and/or supporting information.

ACKNOWLEDGMENTS. We thank Ms. Dejia Guo for sharing technical information about stereotactic viral microinjection. We express our gratitude to Drs. Minmin Luo and Mo Xu for critical reading of the manuscript; Dr. Ting Han for continuous encouragement and critical comments; and Ms. Mengli Shi for drawing the schematic model image. We also thank Drs. Alex Wang and John Hugh Snyder for editorial advice on manuscript preparation. The study was supported by institutional grants from the Ministry of Science and Technology of China, the National Natural Science Foundation of China, and the Beijing Science and Technology Commission.

1. M. Monje *et al*., Roadmap for the emerging field of cancer neuroscience. *Cell [Internet].* **181**, 219–222 (2020). Available from: https://dx.doi.org/10.1016/j.cell.2020.03.034.
2. Y. Hayakawa *et al*., Nerve growth factor promotes gastric tumorigenesis through aberrant cholinergic signaling. *Cancer Cell [Internet].* **31**, 21–34 (2017). Available from: https://dx.doi.org/10.1016/j.ccell.2016.11.005.
3. C. Abe *et al*., C1 neurons mediate a stress-induced anti-inflammatory reflex in mice. *Nat. Neurosci.* **20**, 700–707 (2017).
4. W. Wang *et al*., Age-related dopaminergic innervation augments T helper 2-type allergic inflammation in the postnatal lung. *Immunity [Internet].* **51**, 1102-1118.e7 (2019). Available from: https://doi.org/10.1016/j.immuni.2019.10.002.
5. R. Glaser, J. K. Kiecolt-Glaser, Stress-induced immune dysfunction: implications for health. *Nat. Rev. Immunol.* **5**, 243–251 (2005).
6. E. Maria, V. Reiche, S. Odebrecht, V. Nunes, H. K. Morimoto. Stress, depression, the immune system, and cancer. *Lancet Oncol.* **5**, 617–625 (2004).
7. C. M. Zhao *et al*., Denervation suppresses gastric tumorigenesis. *Sci. Transl. Med.* **6**, 250ra115 (2014).
8. C. Magnon *et al*., Autonomic nerve development contributes to prostate cancer progression. *Science* **341** (2013).
9. R. L. Stornetta, P. G. Guyenet, C1 neurons: A nodal point for stress? *Exp. Physiol.* **103**, 332–336 (2018).
10. P. G. Guyenet *et al*., C1 neurons: The body's EMTs. *Am. J. Physiol. Regul. Integr. Comp. Physiol.* **305**, R187–R204 (2013).
11. Z. Zhao *et al*., A central catecholaminergic circuit controls blood glucose levels during stress. *Neuron* **95**, 138–152.e5 (2017).
12. P. H. Thaker *et al*., Chronic stress promotes tumor growth and angiogenesis in a mouse model of ovarian carcinoma. *Nat. Med.* **12**, 939–944 (2006).
13. E. K. Sloan *et al*., The sympathetic nervous system induces a metastatic switch in primary breast cancer. *Cancer Res.* **70**, 7042–7052 (2010).
14. B. W. Renz *et al*., β2 adrenergic-neurotrophin feedforward loop promotes pancreatic cancer. *Cancer Cell [Internet].* **33**, 75-90.e7 (2018). Available from: https://doi.org/10.1016/j.ccell.2017.11.007.
15. L. M. Pyter, V. Pineros, J. A. Galang, M. K. McClintock, B. J. Prendergast, Peripheral tumors induce depressive-like behaviors and cytokine production and alter hypothalamic-pituitary-adrenal axis regulation. *Proc. Natl. Acad. Sci. U.S.A.* **106**, 9069–9074 (2009).
16. M. D. Goncalves *et al*., High-fructose corn syrup enhances intestinal tumor growth in mice. *Science (80-).* **363**, 1345–1349 (2019).
17. C. M. Hu *et al*., High glucose triggers nucleotide imbalance through O-GlcNAcylation of key enzymes and induces KRAS mutation in pancreatic cells. *Cell Metab. [Internet].* **29**, 1334–1349.e10 (2019). Available from: https://doi.org/10.1016/j.cmet.2019.02.005.
18. G. M. Alexander *et al*., Remote control of neuronal activity in transgenic mice expressing evolved G protein-coupled receptors. *Neuron [Internet].* **63**, 27–39 (2009). Available from: https://dx.doi.org/10.1016/j.neuron.2009.06.014.
19. P. Mombaerts *et al*., RAG-1-deficient mice have no mature B and T lymphocytes. *Cell* **68**, 869–877 (1992).

20. J. Li *et al*., Co-inhibitory molecule B7 superfamily member 1 expressed by tumor-infiltrating myeloid cells induces dysfunction of anti-tumor $CD8^+$ T cells. *Immunity* **48**, 773–786.e5 (2018).
21. S. B. Coffelt *et al*., IL-17-producing γδ T cells and neutrophils conspire to promote breast cancer metastasis. *Nature* **522**, 345–348 (2015).
22. C. Twyman-Saint Victor *et al*., Radiation and dual checkpoint blockade activate non-redundant immune mechanisms in cancer. *Nature* **520**, 373–377 (2015).
23. C. Vanpouille-Box *et al*., TGFβ is a master regulator of radiation therapy-induced antitumor immunity. *Cancer Res.* **75**, 2232–2242 (2015).
24. P. G. R. Burke *et al*., Optogenetic stimulation of adrenergic C1 neurons causes sleep state-dependent cardiorespiratory stimulation and arousal with sighs in rats. *Am. J. Respir. Crit. Care Med.* **190**, 1301–1310 (2014).
25. A. J. Dunn, *The HPA Axis and the Immune System. A Perspective* (NeuroImmune Biology) (2007).
26. M. A. Bellavance, S. Rivest, The HPA—Immune axis and the immunomodulatory actions of glucocorticoids in the brain. *Front. Immunol.* **5**, 136 (2014).
27. F. Q. Wu *et al*., ADRB2 signaling promotes HCC progression and sorafenib resistance by inhibiting autophagic degradation of HIF1α. *J. Hepatol.* **65**, 314–324 (2016).
28. B. Cui *et al*., Stress-induced epinephrine enhances lactate dehydrogenase A and promotes breast cancer stem-like cells. *J. Clin. Invest.* **129**, 1030–1046 (2019).
29. M. M. S. Obradović *et al*., Glucocorticoids promote breast cancer metastasis. *Nature* **567**, 540–544 (2019).
30. H. Yang *et al*., Stress-glucocorticoid-TSC22D3 axis compromises therapy-induced antitumor immunity. *Nat. Med.* **25**, 1428–1441 (2019).
31. Y. Belkaid, T. W. Hand, Role of the microbiota in immunity and inflammation. *Cell* **157**, 121–141 (2014).
32. X. Gao *et al*., Chronic stress promotes colitis by disturbing the gut microbiota and triggering immune system response. *Proc. Natl. Acad. Sci. U.S.A.* **115**, E2960–E2969 (2018).
33. L. Young, J. Sung, G. Stacey, J. R. Masters, Detection of Mycoplasma in cell cultures. *Nat. Protoc.* **5**, 929–934 (2010).
34. T. Tanaka *et al*., A novel inflammation-related mouse colon carcinogenesis model induced by azoxymethane and dextran sodium sulfate. *Cancer Sci.* **94**, 965–973 (2003).
35. C. Neufert, C. Becker, M. F. Neurath, An inducible mouse model of colon carcinogenesis for the analysis of sporadic and inflammation-driven tumor progression. *Nat. Protoc.* **2**, 1998–2004 (2007).